THE JOURNAL OF PHYSICAL CHEMISTRY A

 VOLUME 108, NUMBER 12, MARCH 25, 2004

ARTICLES

Quantum Wave Packet Studies of the $C(^1D) + H_2 \rightarrow CH + H$ Reaction: Integral Cross Section and Rate Constant

Shi Ying Lin and Hua Guo*

Department of Chemistry, University of New Mexico, Albuquerque, New Mexico 87131

Received: October 23, 2003; In Final Form: January 13, 2004

Using a Chebyshev wave packet method, the initial state-specified ($v_i = 0$, $j_i = 0$) integral cross section and rate constant are obtained for the title reaction on the latest version of the ab initio potential energy surface. All partial wave contributions up to $J = 47$ are calculated explicitly within the coupled states (CS) approximation. The resulting integral reaction cross section in the collision-energy range of 0.0−0.5 eV displays an oscillatory structure due to numerous long-lived resonances supported by the deep CH_2 well. The rate constant up to 800 K is nearly temperature-independent except for an initial rise below 100 K. The calculated rate constant at room temperature is in reasonably good agreement with the latest experimental measurement. In addition, exact calculations including the Coriolis coupling have been carried out for three selected partial waves, $J = 2$, 4, and 10. In these Coriolis-coupled calculations, a more accurate and efficient scheme is proposed that allows for a significant reduction of the grid size as well as the spectral range. Comparison with the corresponding CS results indicates that the neglect of the Coriolis coupling leads to the underestimation of the cross section and the rate constant.

I. Introduction

Reactions between atomic carbon and molecular hydrogen play an important role in both combustion[1] and astrochemistry.[2,3] Significant experimental effort has been devoted in the past to the understanding of both kinetic[4−9] and dynamic aspects[9−16] of these reactions. Depending on the electronic character of the carbon atom, the reaction proceeds on different electronic manifolds.[17] In this work, we concentrate on the reaction dynamics involving the singlet of carbon, namely, $C(^1D)$. Its reaction with $H_2(X^1\Sigma_g^+)$ produces $CH(X^2\Pi)$ and $H(^2S)$ and involves at least the first two singlet ($\tilde{a}^1A_1$ and $\tilde{b}^1B_1$) states of CH_2. We note in passing that the reaction between $C(^3P)$ and $H_2(X^1\Sigma_g^+)$ via the triplet manifold has been investigated theoretically by Schatz and co-workers.[18−20]

In addition to its practical importance, the title reaction also serves as a prototype for studying the insertion mechanism, in which the atomic carbon attacks the hydrogen molecule in the perpendicular approach. It is well established that for this reaction there is no barrier for the insertion pathway,[21−23] which leads to the formation of a metastable CH_2 complex supported by a deep potential well. As a result, the reaction dynamics is subjected to the possibly strong influence of long-lived resonance states. In many aspects, this reaction is similar to the more extensively studied $O(^1D) + H_2$ system,[24−39] where the insertion mechanism also predominates at low energies. However, the $C(^1D) + H_2$ reaction is considered[16] to be a "clean" insertion reaction because of its near thermoneutrality and because of a relatively large barrier in the collinear abstraction channel.[21,23]

Stimulated by a recent crossed molecular beam experiment,[16] Launay and co-workers have developed a global potential energy surface (PES) for the lowest-lying singlet ($\tilde{a}^1A_1$) state of the CH_2 system from 1748 multireference singles and doubles

* Corresponding author. E-mail: hguo@unm.edu.

10.1021/jp031184h CCC: $27.50
Published on Web 03/02/2004

configuration interaction (MRSD-CI) points.[23] Unlike earlier near-equilibrium PESs of $CH_2(\tilde{a}^1A_1)$,[40,41] this new PES is global and thus suitable for studying the reaction dynamics of the title system. It predicts no barrier for the insertion pathway leading to the CH_2 well of ~4.3 eV. In the collinear approach, however, a barrier of 0.54 eV essentially blocks the abstraction pathway at low energies. The only potential shortcoming of this PES is the neglect of the Renner−Teller interaction[42] with the $\tilde{b}^1B_1$ state and other non-Born−Oppenheimer interactions that are known to affect the spectroscopy of CH_2.[43−45] Very recently, these ab initio points were refit[46] using the reproducing kernel Hilbert space approach.[47] The new fit removed some spurious features and rendered the PES smoother.

The availability of globally accurate ab initio PESs has stimulated recent theoretical interest in the reaction dynamics. Launay and co-workers have, for example, carried out time-independent quantum studies of the title reaction using the original fit of the PES.[23,48] In particular, the total reaction probability and product internal state distributions for the $C(^1D) + H_2(v_i = 0, j_i = 0)$ reaction ($J = 0$) were reported for collision energies up to 0.5 eV. The energy dependence of the reaction probability showed no threshold and a rich resonance structure, lending strong support to the insertion mechanism. Quantum integral and differential cross sections were later calculated at a single energy point.[48] More recently, we[49] have carried out dynamic and bound-state calculations on the new fit of the PES[46] using a quantum wave packet method. Both reactive and inelastic probabilities for $J = 0$ were obtained. Consistent with the time-independent quantum results,[23] these probabilities were found to be strongly affected by long-lived resonances. From the evolution of the time-dependent wave packet, we also demonstrated unequivocally that the reaction is insertion-dominated. In addition to the quantum work, quasi-classical trajectory calculations have been performed by Banares et al. on both fits of the PES.[46,48] The results agree qualitatively with the averaged quantum mechanical reaction probabilities but lack the fine structure. Reasonably good agreement was also found in cross sections and internal state distributions of the products. Very recently, Manolopoulos and co-workers have analyzed the title reaction using a statistical coupled-channel model, and excellent agreement has been obtained with the quantum differential cross section.[50]

As an extension of our recent work,[49] we in this paper report quantum wave packet calculations of the integral cross section and rate constant for the title reaction on the same PES.[46] The wave packet approach is well suited for computing reaction rates because a single propagation yields the reaction probability at all energies without necessarily the S-matrix elements.[51] In contrast, the traditional time-independent methods will have to repeat the calculation at every energy point. The former is particularly advantageous for reactions that are affected by long-lived resonances, such as the title reaction, in which a fine energy grid is needed. As before, we use in this work the Chebyshev propagator, which bears many similarities to the time propagator. It is accurate and efficient because no approximation of the propagator is needed and because the propagation can be carried out in real space. To obtain the integral cross section, all partial wave contributions spanning from $J = 0$ to 47 were calculated explicitly within the coupled states (CS) approximation. In addition, exact calculations including the Coriolis coupling were carried out for three selected J (= 2, 4, and 10) values to check the accuracy of the CS approximation. The exact calculations were made more efficient and accurate by using a number of novel schemes. Finally, the thermal rate constant over the temperature range of $T = 0-800$ K was calculated with both the CS and estimated exact cross sections and compared with the latest experimental measurement. This paper is organized as follows. In the next section (section II), the relevant theoretical methods and their numerical implementation are outlined. In section III, the calculated results are presented and discussed. Finally in section IV, conclusions are made. Atomic units are used throughout this paper unless otherwise stated.

II. Theory

Following our earlier $J = 0$ work,[49] we use the reactant ($C + H_2$) Jacobi coordinates (R, r, γ) in our calculations. Such a coordinate system allows for the adaptation of the exchange symmetry between the two hydrogen atoms, resulting in reduction of the grid/basis size. The Hamiltonian is expressed as

$$\hat{H} = -\frac{1}{2\mu_R}\frac{\partial^2}{\partial R^2} - \frac{1}{2\mu_r}\frac{\partial^2}{\partial r^2} + \frac{\hat{j}^2}{2\mu_r r^2} + \frac{\hat{l}^2}{2\mu_R R^2} + V(R, r, \gamma) \quad (1)$$

where r and R are respectively the diatomic (H−H) and atom−diatom (C−H_2) distances with μ_r and μ_R as the corresponding reduced masses. $V(R, r, \gamma)$ is the PES. $\hat{j}$ denotes the diatomic rotational angular momentum operator, and $\hat{l}$ denotes the orbital angular momentum operator. $\hat{l}^2$ can be further expressed as

$$\hat{l}^2 \equiv (\hat{J} - \hat{j})^2 = \hat{J}^2 + \hat{j}^2 - 2\hat{J}_z\hat{j}_z - \hat{J}_+\hat{j}_- - \hat{J}_-\hat{j}_+ \quad (2)$$

in which $\hat{J}$ and $\hat{j}$ are respectively the total and diatomic angular momentum operators with $\hat{J}_z$ and $\hat{j}_z$ as their projections onto the body-fixed (BF) z axis. $\hat{J}_+(\hat{J}_-)$ and $\hat{j}_+(\hat{j}_-)$ are the corresponding raising (lowering) operators. In the CS approximation,[52,53] the last two terms in eq 2 will be ignored.

The Chebyshev approach propagates a wave packet using the three-term recursion relationship for the Chebyshev polynomials.[54−63] For scattering problems, the recursion relation is modified by a damping term (D) to enforce the outgoing boundary condition:[57,58]

$$|\psi_{k+1}\rangle = D(2\hat{H}_{\text{norm}}|\psi_k\rangle - D|\psi_{k-1}\rangle) \qquad k > 1 \quad (3)$$

where $|\psi_1\rangle = D\hat{H}_{\text{norm}}|\psi_0\rangle$. The initial wave packet is chosen as the product of a well-defined rovibrational eigenfunction $|\varphi_i\rangle$ and a 1D Gaussian-shaped wave packet along the translational coordinate. In particular, the following form is used:[64]

$$|\psi_0\rangle = N e^{-(R-R_i)^2/2\delta^2}\cos(k_0 R)|\varphi_i\rangle \quad (4)$$

where k_0, R_i, and δ are its central momentum, central position, and width, respectively, and N is the normalization constant. The damping function D is given as a Gaussian-shaped function placed at the edge of the R (and r) grid:

$$D(R) = \begin{cases} 1 & \text{for } R \le R_d \\ e^{-d_R(R-R_d)^2} & \text{for } R > R_d \end{cases} \quad (5)$$

where R_d is the onset of the damping and d_R controls the extent of damping. We note in passing that the propagation in eq 3 can be carried out entirely with real algebra, which represents significant savings over the complex time propagation. The above approach is closely related to the "real wave packet" method of Gray and Balint-Kurti.[64]

In eq 3, the Hamiltonian is properly normalized to avoid divergence in the Chebyshev propagation: $\hat{H}_{\text{norm}} = (\hat{H} - H^+)/H^-$, where $H^{\pm} = (H_{\max} \pm H_{\min})/2$ with $H_{\max}$ ($H_{\min}$) as the upper (lower) spectral bound.[54] This is necessary because of the nonlinear albeit one-to-one mapping between the Chebyshev angle (θ) and the total energy E: $\cos\theta \equiv (E - H^+)/H^-$. Interestingly, this nonlinear mapping allows more interpolation points near both ends of the spectral range, which can be advantageous for the convergence of low-energy spectra or dynamics.[65,66]

Because only final-state-summed information about the reaction is of interest in this work, we take advantage of a flux-based approach that avoids the calculation of S-matrix elements.[67,68] To this end, the initial state-specified total reaction probability is calculated using the following flux-based formula for the Chebyshev propagation:[49,69]

$$P(E) = \frac{1}{2\pi\mu_r |a_i(E)|^2 (H^-)^2 \sin^2\theta} \times \mathrm{Im}\left\langle \sum_k (2 - \delta_{k0}) e^{-ik\theta} \psi_k \right| \times \sum_{k'} (2 - \delta_{k'0}) e^{-ik'\theta} \left[\delta(r - r_f) \frac{\partial}{\partial r} \psi_{k'} \right] \Bigg\rangle \quad (6)$$

where $r = r_f$ defines the dividing surface in the product channel. In the above equation, $a_i(E)$ represents the amplitude of a stationary state at energy E in the initial wave packet, and its value is given by[70]

$$a_i(E) = \left\langle i\sqrt{\frac{\mu_R k_i}{2\pi}} R h_\Lambda^{(2)}(k_i R) \middle| \psi_0 \right\rangle$$

where $h_\Lambda^{(2)}(k_i R)$ is the spherical Hankel function of the second kind.[71] Here, Λ is given by $\Lambda(\Lambda + 1) = J(J + 1) + j_i(j_i + 1) - 2\Omega^2$ in the CS approximation and l in the Coriolis-coupled scheme. The use of Hankel functions allows the placement of the initial wave packet at a sufficiently small R as long as the interaction potential is zero, without concerning the long-range centrifugal terms. (See eq 9 below.)

In the exact calculations, the off-diagonal Coriolis coupling terms decay slowly with R and couple wave packets in different helicity (Ω) channels even at very large R where the interaction potential has long vanished. It is thus advantageous to define the initial wave packet in the space-fixed (SF) frame in which the orbital angular momentum operator is diagonal.[70,72] For exact calculations, therefore, we employ (j_i, l)-specified initial wave packets rather than (j_i, Ω)-specified ones as used in the CS calculations. The SF wave packets are then expanded in terms of the BF basis. Such a choice leads to (j_i, l)-specified reaction probabilities. The same equation for $a_i(E)$ can be used with the substitution of Λ by l. By averaging this probability over all possible l values ($l = |J - j_i|, ..., J + j_i$), one can obtain the j-specified reaction probabilities, which can then be compared with the corresponding CS results. Our approach is thus different from that of Goldfield, Gray, and Meijer,[73,74] who prepared multiple initial wave packets with different Ω values followed by averaging. Our approach allows the initial wave packet to be placed in relatively small R by using the spherical Hankel functions, as discussed above.

The initial state-specified cross section can be obtained in the CS approximation by assembling the initial state-specified (v_i, j_i, Ω) reaction probabilities for various J,

$$\sigma_{v_i j_i}(E_c) = \frac{\pi}{(2j_i + 1)k_i^2} \sum_{J,p,\Omega \le \min(J,j_i)} (2J + 1) P^{Jp}_{v_i j_i \Omega}(E_c) \quad (7)$$

where $k_i^2 = 2\mu_R E_c$, E_c is the collision energy, and $P^{Jp}_{v_i j_i \Omega}(E_c)$ is the initial state ($v_i j_i \Omega$) -specified total reaction probability for the partial wave J and parity p. A similar equation exists for averaging in the SF frame. The initial state-specified rate constant is then given by

$$k_{v_i j_i}(T) = \frac{f}{k_B T}\left(\frac{8}{\pi\mu_R k_B T}\right)^{1/2} \int_0^\infty \sigma_{v_i j_i}(E_c) e^{-E_c/k_B T} E_c \, dE_c \quad (8)$$

where k_B is the Boltzmann constant and f is the electronic degeneracy factor, which is $^1/_5$ for the title reaction.[17]

The major computational task in our approach is the matrix−vector multiplication (namely, $\hat{H}\psi$) entailed by eq 3. In this work, a mixed representation is employed to discretize the Hamiltonian and wave packet. In the CS approximation, the Coriolis coupling terms in eq 2 are ignored, rendering the conservation of $\hat{J}_z$ and $\hat{j}_z$. Hence, their common eigenvalue, denoted by Ω, is a good quantum number. Such an approximation greatly simplifies $J > 0$ calculations both in view of the computational effort and numerical implementation and provides reasonably accurate results for many reactions. To that end, the only additional term in the Hamiltonian for $J > 0$ is in the form of a centrifugal potential:

$$\hat{H}^J = \hat{H}^{J=0} + \frac{J(J + 1) - 2\Omega^2}{2\mu_R R^2} \quad (9)$$

As a result, the numerical implementation is essentially the same as that of $J = 0$. As in our previous work,[49] a direct product discrete variable representation (DVR)[75] is used for the three internal degrees of freedom (R, r, γ). The overall rotation is represented by the Wigner rotation matrix[76] ($D^J_{\Omega,M}$) with the adaptation of parity (p):

$$|JM\Omega p\rangle = (2 + 2\delta_{\Omega,0})^{-1/2}(|JM\Omega\rangle + p(-1)^{J+\Omega}|JM - \Omega\rangle) \quad (10)$$

where

$$|JM\Omega\rangle = \sqrt{\frac{2J+1}{8\pi^2}} D^{J*}_{\Omega,M}$$

In the CS approximation, the angular kinetic energy operators (KEOs) are diagonal with respect to J, Ω, and M, which appear only as parameters. Without the loss of generality, $M = 0$ is taken. In this case, the Wigner rotation matrix is reduced to an associate Legendre function.

In the Coriolis-coupled treatment, however, Ω is no longer a good quantum number. The coupling between different Ω channels represents an additional degree of freedom at nonzero Js and results in increased computational effort that is proportional to J. As in the CS model, the two radial degrees of freedom (R, r) are discretized in a direct product DVR. However, a finite basis representation (FBR) is used for the angular degrees of freedom. In particular, the wave packet is expanded in the mixed DVR/FBR representation,

$$|\psi\rangle^{Jp} = \sum \psi^{Jp}_{\alpha_1\alpha_2 j\Omega} |\alpha_1\alpha_2\rangle |j\Omega; Jp\rangle \quad (11)$$

where α_1 and α_2 denote the grid indices along the R and r coordinates, respectively. The angular FBR in the above equation is defined as follows:

$$|j\Omega; Jp\rangle = (2 + 2\delta_{\Omega,0})^{-1/2}(|J\Omega\rangle|j\Omega\rangle + p(-1)^J|J - \Omega\rangle|j - \Omega\rangle) \quad (12)$$

where $|j\Omega\rangle \equiv \Theta_{j\Omega}(\gamma, 0)$ are normalized associated Legendre functions with the Condon−Shortley phase convention[77] and Ω is restricted to nonnegative values. In this basis, all KEOs are diagonal except for the Coriolis coupling term, which is tri-diagonal. In particular,

$$\langle j'\Omega'; Jp|\hat{j}^2|j\Omega; Jp\rangle = j(j + 1)\delta_{j',j}\delta_{\Omega',\Omega} \quad (13a)$$

$$\langle j'\Omega'; Jp|\hat{l}^2|j\Omega; Jp\rangle = [J(J + 1) + j(j + 1) - 2\Omega^2]\delta_{j',j}\delta_{\Omega',\Omega} - [(1 + \delta_{\Omega',0})(1 + \delta_{\Omega,0})]^{-1/2}\{\lambda^+_{J\Omega}\lambda^+_{j\Omega}\delta_{\Omega',\Omega+1} + \lambda^-_{J\Omega}\lambda^-_{J\Omega}[\delta_{\Omega',\Omega-1} + p(-1)^J\delta_{\Omega',-\Omega+1}]\}\delta_{j',j} \quad (13b)$$

where $\lambda^{\pm}_{jm} = \sqrt{j(j + 1) - m(m \pm 1)}$. Because Ω and Ω' are restricted to nonnegative values, the term associated with parity in eq 13b survives only for $\Omega = 0, 1$.

The use of FBR simplifies the rotational KEOs but complicates the calculation of the action of the potential energy operator. However, the latter can be performed efficiently using the following pseudo-spectral transformation:[78,79]

$$T^{(\Omega)}_{j\beta} = \sqrt{w_\beta}\Theta_{j\Omega}(\gamma_\beta) \quad (14)$$

where β denotes the index of the Gauss−Legendre quadrature points for the internal angular coordinate and w_β is the corresponding weight.

Because of the insertion nature of the title reaction, the wave packet can easily access regions near $R = 0$. Even without the explicit inclusion of the singularity, population near it can result in a very large spectral range. To alleviate this problem, we use a scheme to restrict the spectral range of the rotational KEOs at small R. In particular, the BF-FBR $|j\Omega; Jp\rangle$ is first transformed to the SF-FBR $|jl; Jp\rangle$ using the following equation,[51,72]

$$|j\Omega; Jp\rangle = \sum_l (-1)^{j-l+\Omega}\sqrt{(2 - \delta_{\Omega,0})(2l + 1)}\begin{pmatrix} j & l & J \\ \Omega & 0 & -\Omega \end{pmatrix}|jl; Jp\rangle \quad (15)$$

where (:::) denotes the 3-j symbol. Because the rotational KEOs are diagonal in the SF-FBR, the spectral range can be easily controlled by truncating the rotational energy. After applying the truncated rotational KEOs, the wave function is transformed back to the original BF-FBR. The drawback of this method is that it is slightly more expensive to compute the matrix−vector multiplication.

III. Results and Discussion

As in our earlier work,[49] equidistant grids with $N_R = 188$ and $N_r = 79$ points were used for the two radial coordinates in the ranges of $R \in [0,16.0]a_0$ and $r \in [0.5,12.0]a_0$, respectively. The fast sine Fourier transform was used to calculate the action of the radial KEOs on the propagating wave packet.[80] For the Jacobi angle, 25 Gauss−Legendre quadrature points were taken between $\gamma = \pi/2$ and π, which corresponds to $j_{max} = 48$. Only *para*-H_2 was considered in this work, and thus only even j states were included. Both the potential and the angular KEOs[81] were truncated at 0.5 hartree to minimize the spectral range.

The initial wave packet was launched at $R_i = 8.0a_0$ with $\delta = 0.3a_0$, and the initial momentum was chosen to give an averaged collision energy of 0.15 eV. As noted in the previous section, (j_i, Ω)-specified initial wave packets were used in CS calculations, and (j_i, l)-specified ones were used in Coriolis-coupled calculations. Because of the requirement for $j_i \geq \Omega \geq 0$, Ω is restricted to be zero in the CS calculations because of $j_i = 0$. However, in the exact calculations, Ω is a variable spanning from $\Omega = 0$ to J, and because j_i is 0, l has only one value ($l = J$). The onset of damping was placed at $R_d = 11.0a_0$ and $r_d = 8.0a_0$ with the damping coefficients $d_R = 0.0005a_0^{-1}$ and $d_r = 0.004a_0^{-1}$, respectively. The flux was calculated at $r_f = 6.9a_0$. The number of Chebyshev propagation steps that was found to be sufficient to converge the reaction probabilities up to 0.5 eV was 50 000. When comparing with the O + H_2 system,[25,27,28,30] we found that our calculations require a much larger number of propagation steps to resolve the resonance structure, although the size of our grid is somewhat smaller.

A. Accuracy of CS Approximation. The CS approximation has been widely used to study reaction dynamics. In many cases, it has been shown to be quite accurate. For instance, Carroll and Goldfield studied the reaction probability of the O(^{1}D) + H_2 reaction and concluded that the errors introduced by the CS approximation are small.[36] However, there is also ample evidence that the Coriolis coupling can be quite significant in some other systems. Indeed, Meijer and Goldfield have found that the neglect of Coriolis coupling results in significant errors in the H + O_2 reaction probabilities.[82] Because the results presented below are mainly from the CS calculations, it is important to assess the accuracy of the CS approximation for the C(^{1}D) + H_2 reaction.

To this end, we have performed exact Coriolis-coupled calculations for $J = 2$, 4, and 10. The results are compared with the CS model in Figure 1. In the left panels, the comparison between the exact and CS reaction probabilities indicates that they are in qualitatively good agreement: both show rich resonance structures with comparable backgrounds and thresholds. However, quantitative differences, such as peak positions, do exist. Overall, the exact probabilities appear to be larger, particularly at large Js. To estimate the error in the CS approximation in the more averaged rate constant, the following quantity is compared in the right panels of Figure 1,

$$P^J(T) = \int_0^\infty P^J(E_c)e^{-E_c/k_BT}\,dE_c \quad (16)$$

where $P^J(E_c)$ is the reaction probability of the Jth partial wave as defined in eq 6, which is obtainable from both the exact and CS calculations. Similarly, $P^J(T)$ represents the Jth partial wave contribution to the rate constant. As shown in the figure, the two results are in reasonable agreement both in absolute magnitude and temperature dependence. Quantitatively, however, the CS model consistently underestimates, and the relative error is larger at larger Js and lower temperatures. For $J = 2$, for example, the CS results underestimate by 7.4 and 3.6% at $T = 300$ and 800 K, respectively. For $J = 4$, the error increases to 16.9 and 12.3%, respectively. At the highest J (= 10) calculated, the error are 26.4 and 24.0%, respectively. These results suggest that the CS approximation should provide a reasonable rate constant. However, quantitative errors can be quite significant. This issue will be revisited below when the integral cross section and rate constant are presented.

B. Reaction Probabilities. The energy dependence of the total reaction probability obtained from the CS approximation

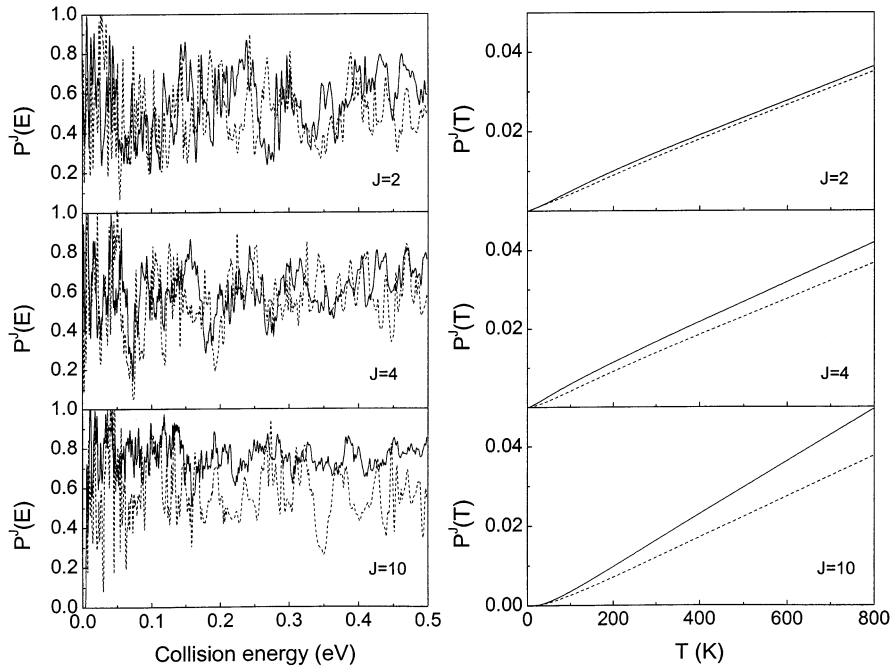

Figure 1. Comparison of initial state ($v_i = 0$, $j_i = 0$)-specified reaction probabilities ($P^J(E)$) and contributions to the thermal rate constant ($P^J(T)$) between the CS (- - -) and exact (—) models.

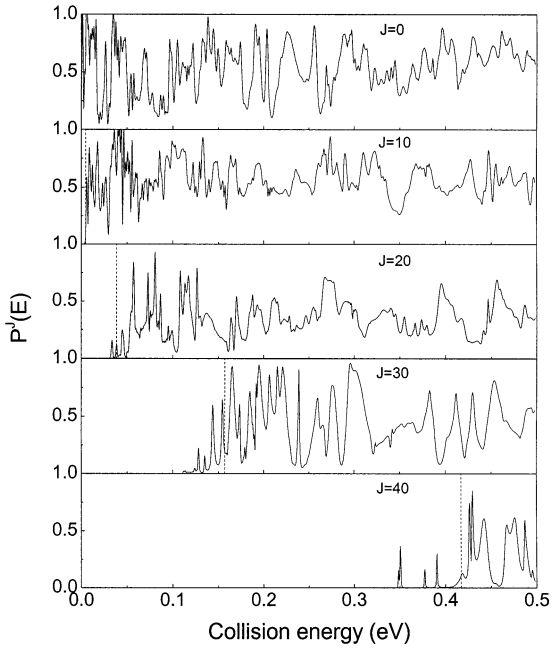

Figure 2. Initial state ($v_i = 0$, $j_i = 0$) -specified CS reaction probabilities at different J values. The reaction thresholds calculated from the classical centrifugal barrier heights are indicated by vertical dashed lines.

is displayed in Figure 2 for a number of total angular momentum quantum numbers (J). Several observations are immediate. First, the probability for $J = 0$ has no threshold. As discussed in earlier work,[23,49] this is consistent with the barrierless insertion pathway that dominates the reaction. Second, all of the probabilities show oscillatory structures superimposed on broad backgrounds. The oscillation is particularly strong near the corresponding reaction threshold but becomes less pronounced at higher energies, presumably because of shorter resonance lifetimes. The sharp peaks can be attributed to long-lived resonances in the CH_2 well, as discussed in the previous $J = 0$ work.[23,49] Obviously, a better understanding of these resonances is of great interest and will be discussed in a future publication. Comparing with the O(^{1}D) + H_2 reaction,[25,30] we found that average reaction probabilities are significantly smaller at all J values. This can be attributed to the much smaller exothermicity in the title reaction, which results in substantial nonreactive (elastic and inelastic) scattering. The situation here is somewhat similar to the endothermic C(^{3}P) + H_2 reaction.[19]

For low Js, the reaction probability at very low kinetic energy cannot be accurately determined because of the damping of the propagating wave packet on a finite grid. Sometimes the reaction probability can exceed unity, a clearly unphysical outcome. However, such a deficiency does not affect the cross section and rate constant in a significant way.

Another clear trend observable in Figure 2 is that the reaction threshold shifts to higher energy as J increases. This is due to the increase in the J-dependent centrifugal barrier for this intrinsically barrierless reaction. This shift of the reaction threshold with J can be approximately described by J-shifting[83] or capture models.[30,84] The classical capture model is based on the premise that all trajectories react if they manage to overcome the centrifugal barrier along the reaction path. A more sophisticated quantum version proposed by Gray et al. uses the height of the centrifugal barrier at $\bar{l} = \bar{J} - \bar{j}_i$ to shift the reaction probability.[30] Indeed, such an approach has worked quite well for the insertion-dominated O(^{1}D) + H_2 reaction.

In Figure 3, the effective potential barrier height along R is given for different total angular momentum quantum numbers (J), which in our case is equal to l because $j_i = 0$. The barrier is defined as the highest point on the 1D effective potential in the R coordinate with optimization in (r, γ) space. It can be readily seen that there are two regions of J dependence. At low J, the barrier is located somewhere in $R \in [6, 10]a_0$. Above $J = 25$, another barrier at a smaller R (≈ 3 Å) takes over. The inner barrier originates from a shoulder in the entrance channel potential, and its smaller C−H_2 distance results in a sharper J dependence. The barrier height can be used to predict the classical reaction threshold at the corresponding J. As shown in Figure 2 with vertical dashed lines, the predicted thresholds are reasonably accurate. An anomaly is some sharp peaks below

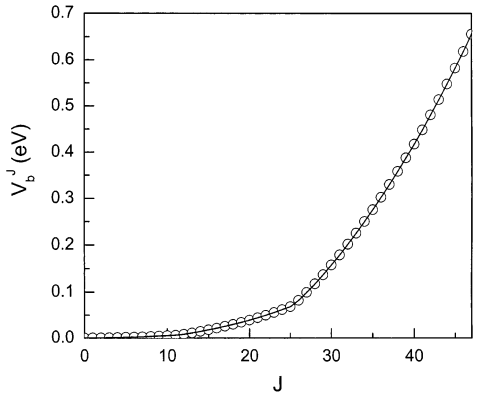

Figure 3. Dependence of the classical centrifugal barrier height on *J*.

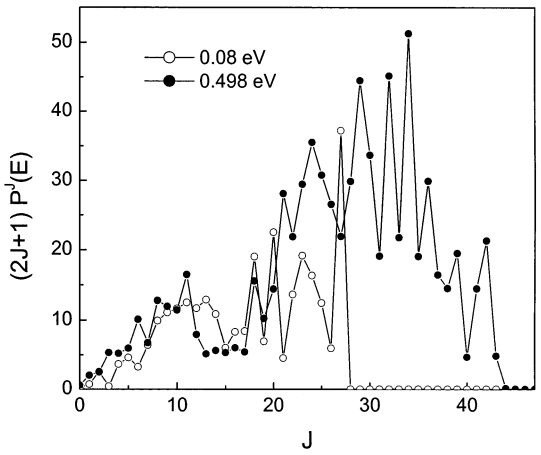

Figure 4. Weighted CS partial wave contributions to the integral cross section at $E_c = 0.08$ (○) and 0.498 eV (●).

the classical threshold at large *J*. These isolated peaks are likely to be the results of long-lived resonances. Their contributions to reactivity are presumably facilitated by tunneling and/or smaller zero-point energy near the classical barrier.

C. Integral Cross Section. The integral reaction cross section is a sum of weighted reaction probabilities over many partial waves, according to eq 7. At a given energy, the partial wave contribution usually increases with *J* initially because of the $(2J + 1)$ degeneracy factor and subsequently decreases with *J* because of the shift of the reaction threshold to higher energies. This is clearly shown in Figure 4 for $E_c = 0.08$ and 0.498 eV within the CS approximation. The oscillatory structures in the *J*-dependence of partial wave contributions are associated with the resonances as discussed above. The figure also illustrates the fact that the higher the collision energy the more partial waves are needed. Within the CS model, the inclusion of partial wave contributions up to $J = 44$ is sufficient to converge the cross section below 0.5 eV. As a result, we have included all the partial wave contributions up to $J = 47$.

The integral reaction cross section obtained within the CS approximation is displayed in Figure 5 (dashed line) for E_c up to 0.5 eV. It shows that the cross section has no threshold, as can be expected from the zero barrier of the PES. The oscillatory structure notwithstanding, the cross section is very large near zero collision energy and decreases sharply with the increase in E_c. Above 0.1 eV, the cross section levels off and eventually reaches about 5 Å^2 at $E_c = 0.5$ eV. The energy dependence of the cross section is very similar to that of the insertion-dominated $O(^1D) + H_2$ reaction.[25,29,30]

The quantum CS cross section can be compared with previous classical results using the same PES.[46] Despite the absence of

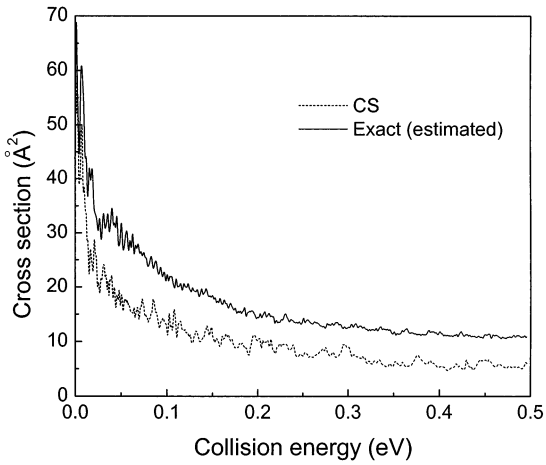

Figure 5. Initial state ($v_i = 0$, $j_i = 0$) -specified integral cross sections from the CS (- - -) and exact (—) reaction probabilities estimated from a capture model.

oscillatory structure, the classical cross section also shows an initial drop at low collision energies and a slower decay at higher energies. Quantitatively, however, it is generally larger than the CS cross section over the energy range studied in this work except for very low energies. At $E_c = 0.08$ eV, for example, the quantum CS cross section is 13.6 Å^2, which can be compared with the classical value of 22.5 Å^2. The CS value is also significantly smaller than the only available exact quantum cross section of 30.5 Å^2 at the same collision energy, obtained using a time-independent method.[48] Of course, the comparison at a single energy point can be a little misleading because of the oscillatory quantum cross section. However, even the averaged CS cross section near 0.08 eV (15.5 Å^2) is still much less than the classical or the exact quantum value. At higher collision energies, 0.5 eV for example, the CS cross section (5.7 Å^2) is also smaller than the classical one (∼11 Å^2).[46]

We attribute the above discrepancies to the neglect of Coriolis coupling in the CS model. As shown in Figure 1, reaction probabilities in the CS model systematically underestimate, particularly at large *J*. If this trend persists at larger *J*s, it is not difficult to understand the underestimation of the cross section by the CS model at $E_c = 0.08$ eV because the partial waves with $J \geq 10$ make significant contributions, as shown in Figure 4. To resolve this issue unequivocally, exact calculations at higher *J*s need be carried out.

To estimate the exact cross section and its energy dependence, we adopted a capture model proposed by Gray and co-workers.[30] To this end, the reaction probability of a particular total angular momentum *J* is estimated from that of an explicitly calculated one at J_1 ($J \geq J_1$):

$$P^J(E) = P^{J_1}(E - V_b^J + V_b^{J_1}) \tag{17}$$

where V_b^J denotes the classical centrifugal barrier height for *J* as shown in Figure 3. If reaction probabilities for two different angular momentum quantum numbers (J_1 and J_2) are available, then a more reasonable estimate can be obtained for the *J* ($J_1 < J < J_2$) values in between by interpolation:[72]

$$P^J(E) = \frac{J_2 - J}{J_2 - J_1} P^{J_1}(E - V_b^J + V_b^{J_1}) + \frac{J - J_1}{J_2 - J_1} P^{J_2}(E - V_b^J + V_b^{J_2}) \tag{18}$$

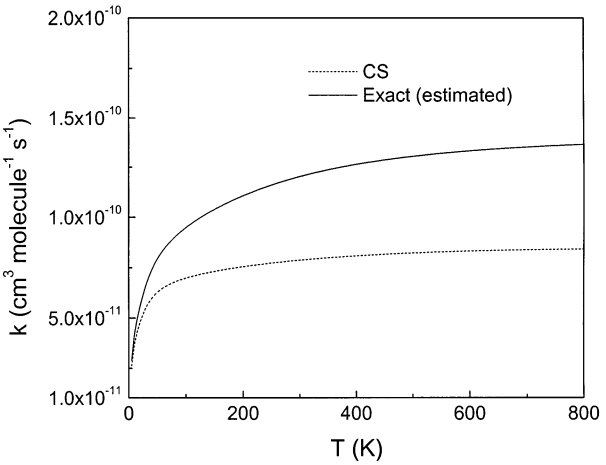

Figure 6. Initial state ($v_i = 0$, $j_i = 0$)-specified rate constants calculated from the CS (- - -) and estimated exact (—) cross sections.

As discussed above, the rationale for the capture model is based on the observation that the reactivity of this barrierless reaction is primarily determined by the centrifugal barrier in the entrance channel.

The resulting cross section is plotted in Figure 5 with a solid line. It is quite clear from the figure that the estimated exact cross section is larger than the CS cross section throughout the energy range. At $E_c = 0.08$ eV, for example, the estimated exact cross section is 23.8 Å^2, which is in much better agreement with the previous quantum and classical values (30.5 and 22.5 Å^2, respectively). Similarly, at $E_c = 0.5$ eV, our result (10.8 Å^2) is in reasonably good agreement with the classical cross section (~11 Å^2). Given the importance of $J > 10$ partial waves as shown in Figure 4, it is conceivable that better agreement can be reached if the Coriolis-coupled calculations can be extended to larger *J*s. However, such a numerically intensive task is beyond the scope of this work.

Interestingly, the CS approximation has been shown to be quite accurate in the O(^{1}D) + H_2 reaction.[36] As extensively discussed in the literature,[25,28,30] the O(^{1}D) + H_2 reaction has near-unity reactivity at small *J* values because of its large exothermicity. The success of the capture model in that system further indicates that the reactivity is controlled by a long-range centrifugal barrier in the reactant channel, where the CS approximation is expected to work well, rather than long-lived resonances in the deep H_2O well. In the C(^{1}D) + H_2 system, however, the insertion of atomic carbon into the hydrogen molecule leads to significant inelastic scattering and only partial reaction. In addition, both scattering processes are strongly affected by long-lived resonances. The CS approximation based on *R* embedding is expected to perform poorly in the CH_2 complex well and the product channel. Hence, the relatively large errors in the CS model probably stem from the dominance of long-lived resonances in the title system.

D. Rate Constant. The initial state ($v_i = 0$, $j_i = 0$) specific thermal rate constant up to 800 K has been calculated using both the CS and estimated exact cross sections discussed above. As displayed in Figure 6, the rate from the CS cross section is somewhat smaller than that from the estimated exact cross section based on the capture model. Both rate constants show a sharp increase at lower temperatures. Above 100 K, however, the rate becomes nearly temperature-independent. This is consistent with the barrierless nature of the insertion reaction. Unfortunately, there is no experimental data on the temperature dependence of the rate constant.

The calculated rate constants can be compared with experimental measurements at room temperature (300 K). The rates from the CS and the estimated exact cross sections are 0.7×10^{-10} and 1.2×10^{-10} cm^3 molecule^{-1} s^{-1}, respectively. They are in reasonable agreement with the latest experimental value of $(2.0 \pm 0.6) \times 10^{-10}$ cm^3 molecule^{-1} s^{-1}.[9] The agreement with the experimental value should be viewed in the context that the calculated rate constants are for a particular initial state ($v_i = 0$, $j_i = 0$). A thermal average over the initial rotational states may modify the picture. In addition, errors in the PES and the neglect of nonadiabatic couplings such as the Renner−Teller effect as well as errors in dynamic treatments represent other factors that may affect the results.

IV. Conclusions

The major objective of this work is to compute an initial state-specified integral cross section and rate constant for the C(^{1}D) + H_2 reaction. To this end, we have explicitly calculated within the CS approximation reaction probabilities over $E_c = 0.0-0.5$ eV for *J* up to 47, which allowed us to compute the reaction cross section in the same energy range and the thermal rate constant in $T = 0-800$ K. The calculated initial state-specific rate is shown to be nearly temperature-independent above 100 K. It agrees reasonably well with the measured experimental rate constant at room temperature.

To assess the accuracy of the CS model in this system, we have performed exact calculations for $J = 2$, 4, and 10. Comparisons at these limited *J* values indicate that Coriolis coupling is quite significant despite the qualitative validity of the CS model. In particular, the CS model consistently underestimates the exact cross section and rate. On the basis of a capture model, we have estimated the integral reaction cross section and rate constant using the exact reaction probabilities at limited *J* values. The results show a significant improvement in agreement with previous classical, exact quantum, and experimental data. The errors introduced by the CS approximation are much more significant than those in the O(^{1}D) + H_2 reaction, which are attributed to the dominance of the long-lived resonances in the title system.

The calculations reported in this work were carried out using an efficient Chebyshev wave packet propagation method. This system represents a challenge because of the large number of long-lived resonances that strongly affect the reactivity in this system. Several novel implementations have been proposed and used to make the calculation more accurate and efficient. In particular, an SF-based scheme is used in preparing the initial wave packet and in its propagation, which allows a smaller grid and better control of the spectral range in the Coriolis-coupled calculations.

Acknowledgment. This work was supported by the National Science Foundation (CHE-0090945). We thank Evi Goldfield, Stephen Gray, David Manolopoulos, Anthony Meijer, George Schatz, and John Zhang for useful discussions and Gabriel Balint-Kurti and David Manolopoulos for sending us their work prior to publication.

References and Notes

(1) Gaydon, A. G. *The Spectroscopy of Flames*; Chapman and Hall: London, 1974.

(2) Flower, D. R.; PineaudesForêts, G. *Mon. Not. R. Astron. Soc.* **1998**, *297*, 1182.

(3) Bucher, M. E.; Glinski, R. J. *Mon. Not. R. Astron. Soc.* **1999**, *308*, 29.

(4) Braun, W.; Bass, A. M.; Davis, D. D.; Simmons, J. D. *Proc. Royal Soc. London, Ser. A* **1969**, *312*, 417.
(5) Husain, D.; Kirsch, L. J. *Chem. Phys. Lett.* **1971**, *9*, 412.
(6) Husain, D.; Norris, P. E. *Faraday Discuss.* **1979**, *67*, 273.
(7) Becker, K. H.; Engelhardt, B.; Wiesen, P.; Bayes, K. D. *Chem. Phys. Lett.* **1989**, *154*, 342.
(8) Dean, A. J.; Davidson, D. F.; Hanson, R. K. *J. Phys. Chem.* **1991**, *95*, 183.
(9) Sato, K.; Ishida, N.; Kurakata, T.; Iwasaki, A.; Tsuneyuki, S. *Chem. Phys. Lett.* **1998**, *237*, 195.
(10) Jursich, G. M.; Wiesenfeld, J. R. *Chem. Phys. Lett.* **1984**, *110*, 14.
(11) Jursich, G. M.; Wiesenfeld, J. R. *J. Chem. Phys.* **1985**, *83*, 910.
(12) Fisher, W. H.; Carrington, T.; Sadowski, C. M.; Dugan, C. H. *Chem. Phys.* **1985**, *97*, 433.
(13) Scott, D. C.; deJuan, J.; Robie, D. C.; Schwartz-Lavi, D.; Reisler, H. *J. Phys. Chem.* **1992**, *96*, 2509.
(14) Mikulecky, K.; Gericke, K.-H. *J. Chem. Phys.* **1993**, *98*, 1244.
(15) Scholefield, M. R.; Goyal, S.; Choi, J.-H.; Reisler, H. *J. Phys. Chem.* **1995**, *99*, 14605.
(16) Bergeat, A.; Cartechini, L.; Balucani, N.; Capozza, G.; Philips, L. F.; Casavecchia, P.; Volpi, G. G.; Bonnet, L.; Rayez, J.-C. *Chem. Phys. Lett.* **2000**, *327*, 197.
(17) Bearda, R. A.; vanHemert, M. C.; vanDishoeck, E. F. *J. Chem. Phys.* **1992**, *97*, 8240.
(18) Harding, L. B.; Guadagnini, R.; Schatz, G. C. *J. Phys. Chem.* **1993**, *97*, 5472.
(19) Guadagnini, R.; Schatz, G. C. *J. Phys. Chem.* **1993**, *100*, 5472.
(20) vanHarrevelt, R.; vanHemert, M. C.; Schatz, G. C. *J. Chem. Phys.* **2002**, *116*, 6002.
(21) Blint, R. J.; Newton, M. D. *Chem. Phys. Lett.* **1975**, *32*, 178.
(22) Whitlock, P. A.; Muckerman, J. T.; Kroger, P. M. In *Potential Energy Surfaces and Dynamical Calculations*; Truhlar, D. G., Ed.; Plenum: New York, 1981.
(23) Bussery-Honvault, B.; Honvault, P.; Launay, J.-M. *J. Chem. Phys.* **2001**, *115*, 10701.
(24) Ho, T.-S.; Hollebeek, T.; Rabitz, H.; Harding, L. B.; Schatz, G. C. *J. Chem. Phys.* **1996**, *105*, 10472.
(25) Peng, T.; Zhang, D. H.; Zhang, J. Z. H.; Schinke, R. *Chem. Phys. Lett.* **1996**, *248*, 37.
(26) Varandas, A. J. C.; Voronin, A. I.; Riganelli, A.; Caridade, P. J. S. B. *Chem. Phys. Lett.* **1997**, *278*, 325.
(27) Dai, J. *J. Chem. Phys.* **1997**, *107*, 4934.
(28) Balint-Kurti, G. G.; Gonzalez, A.; Goldfield, E. M.; Gray, S. K. *Faraday Discuss.* **1998**, *110*, 169.
(29) Drukker, K.; Schatz, G. C. *J. Chem. Phys.* **1999**, *111*, 2451.
(30) Gray, S. K.; Goldfield, E. M.; Schatz, G. C.; Balint-Kurti, G. G. *Phys. Chem. Chem. Phys.* **1999**, *1*, 1141.
(31) Gray, S. K.; Petrongolo, C.; Drukker, K.; Schatz, G. C. *J. Phys. Chem. A* **1999**, *103*, 9448.
(32) Gray, S. K.; Balint-Kurti, G. G.; Schatz, G. C.; Lin, J. J.; Liu, X.; Harich, S.; Yang, X. *J. Chem. Phys.* **2000**, *113*, 7330.
(33) Hankel, M.; Balint-Kurti, G. G.; Gray, S. K. *J. Chem. Phys.* **2000**, *113*, 9658.
(34) Liu, X.; Lin, J. J.; Harich, S.; Schatz, G. C.; Yang, X. *Science* **2000**, *289*, 1536.
(35) Hankel, M.; Balint-Kurti, G. G.; Gray, S. K. *J. Phys. Chem. A* **2001**, *105*, 2330.
(36) Carroll, T. E.; Goldfield, E. M. *J. Phys. Chem. A* **2001**, *105*, 2251.
(37) Honvault, P.; Launay, J.-M. *J. Chem. Phys.* **2001**, *114*, 1057.
(38) Takayanagi, T. *J. Chem. Phys.* **2002**, *116*, 2439.
(39) Aoiz, F. J.; Banares, L.; Castillo, J. F.; Herrero, V. J.; Martinez-Haya, B.; Honvault, P.; Launay, J.-M.; Liu, X.; Lin, J. J.; Harich, S.; Wang, C. C.; Yang, X. *J. Chem. Phys.* **2002**, *116*, 10692.
(40) Comeau, D. C.; Shavitt, I.; Jensen, P.; Bunker, P. R. *J. Chem. Phys.* **1989**, *90*, 6491.
(41) Green, W. H.; Handy, N. C.; Knowles, P. J.; Carter, S. *J. Chem. Phys.* **1991**, *94*, 118.
(42) Renner, E. *Z. Phys.* **1934**, *92*, 172.
(43) Petek, H.; Nesbitt, D. J.; Darwin, D. C.; Ogilby, P. R.; Moore, C. B. *J. Chem. Phys.* **1989**, *91*, 6566.
(44) Chang, B.-C.; Wu, M.; Hall, G. E.; Sears, T. J. *J. Chem. Phys.* **1994**, *101*, 9236.
(45) Hartland, G. V.; Qin, D.; Dai, H.-L. *J. Chem. Phys.* **1995**, *102*, 6641.
(46) Banares, L.; Aoiz, F. J.; Vazquez, S. A.; Ho, T.-S.; Rabitz, H. *Chem. Phys. Lett.* **2003**, *374*, 243.
(47) Hollebeek, T.; Ho, T.-S.; Rabitz, H. *Annu. Rev. Phys. Chem.* **1999**, *50*, 537.
(48) Banares, L.; Aoiz, F. J.; Honvault, P.; Bussery-Honvault, B.; Launay, J.-M. *J. Chem. Phys.* **2003**, *118*, 565.
(49) Lin, S. Y.; Guo, H. *J. Chem. Phys.* **2003**, *119*, 11602.
(50) Rackham, E. J.; Gonzalez-Lezana, T.; Manolopoulos, D. E. *J. Chem. Phys.* **2003**, *119*, 12895.
(51) Zhang, J. Z. H. *Theory and Application of Quantum Molecular Dynamics*; World Scientific: Singapore, 1999.
(52) Pack, R. T. *J. Chem. Phys.* **1974**, *60*, 633.
(53) McGuire, P.; Kouri, D. J. *J. Chem. Phys.* **1974**, *60*, 2488.
(54) Tal-Ezer, H.; Kosloff, R. *J. Chem. Phys.* **1984**, *81*, 3967.
(55) Huang, Y.; Zhu, W.; Kouri, D. J.; Hoffman, D. K. *Chem. Phys. Lett.* **1993**, *214*, 451.
(56) Huang, Y.; Kouri, D. J.; Hoffman, D. K. *Chem. Phys. Lett.* **1994**, *225*, 37.
(57) Mandelshtam, V. A.; Taylor, H. S. *J. Chem. Phys.* **1995**, *102*, 7390.
(58) Mandelshtam, V. A.; Taylor, H. S. *J. Chem. Phys.* **1995**, *103*, 2903.
(59) Chen, R.; Guo, H. *J. Chem. Phys.* **1996**, *105*, 3569.
(60) Kroes, G.-J.; Neuhauser, D. *J. Chem. Phys.* **1996**, *105*, 8690.
(61) Althorpe, S. C.; Kouri, D. J.; Hoffman, D. K. *J. Chem. Phys.* **1997**, *106*, 7629.
(62) Chen, R.; Guo, H. *Comput. Phys. Commun.* **1999**, *119*, 19.
(63) Lin, S. Y.; Guo, H. *J. Chem. Phys.* **2002**, *117*, 5183.
(64) Gray, S. K.; Balint-Kurti, G. G. *J. Chem. Phys.* **1998**, *108*, 950.
(65) Chen, R.; Guo, H. *J. Chem. Phys.* **1998**, *108*, 6068.
(66) Chen, R.; Guo, H. *J. Chem. Phys.* **2003**, *119*, 5762.
(67) Neuhauser, D.; Baer, M.; Judson, R. S.; Kouri, D. J. *J. Chem. Phys.* **1990**, *93*, 312.
(68) Zhang, D. H.; Zhang, J. Z. H. *J. Chem. Phys.* **1994**, *101*, 1146.
(69) Meijer, A. J. H. M.; Goldfield, E. M.; Gray, S. K.; Balint-Kurti, G. G. *Chem. Phys. Lett.* **1998**, *293*, 270.
(70) Althorpe, S. C. *J. Chem. Phys.* **2001**, *114*, 1601.
(71) Messiah, A. *Quantum Mechanics*; Wiley: New York, 1968.
(72) Balint-Kurti, G. G. *Adv. Chem. Phys.* **2004**, *128*, 249.
(73) Goldfield, E. M.; Gray, S. K. *Comput. Phys. Commun.* **1996**, *98*, 1.
(74) Meijer, A. J. H. M.; Goldfield, E. M. *J. Chem. Phys.* **1998**, *108*, 5404.
(75) Light, J. C.; Carrington, T. *Adv. Chem. Phys.* **2000**, *114*, 263.
(76) Zare, R. N. *Angular Momentum*; Wiley: New York, 1988.
(77) Condon, E. U.; Shortley, G. H. *The Theory of Atomic Spectra*; Cambridge: London, 1964.
(78) Corey, G. C.; Lemoine, D. *J. Chem. Phys.* **1992**, *97*, 4115.
(79) Corey, G. C.; Tromp, J. W. *J. Chem. Phys.* **1995**, *103*, 1812.
(80) Kosloff, D.; Kosloff, R. *J. Comput. Phys.* **1983**, *52*, 35.
(81) Ma, G.; Guo, H. *J. Chem. Phys.* **1999**, *111*, 4032.
(82) Meijer, A. J. H. M.; Goldfield, E. M. *J. Chem. Phys.* **1999**, *110*, 870.
(83) Bowman, J. M. *J. Phys. Chem.* **1991**, *95*, 4960.
(84) Clary, D. C. *Mol. Phys.* **1984**, *53*, 3.